Digest Journal of Nanomaterials and Biostructures Vol. 14, No.2, April - June 2019, p. 447 - 461

THE EFFECTS OF TARGETS' PREPARATION CONDITIONS ON THE BIOACTIVITY AND PHYSICAL PROPERTIES OF ABLATED HYDROXYAPATITE BY PULSED LASER

D. M. NASER[a], M. SH. ALHILFI[a,*], N. J. MOHAMMED[b]
[a]*Physics department/Education college/ Mustansiriya University-Iraq*
[b]*Physics department/Science college/ Mustansiriya University-Iraq*

Pulse laser ablation of solids in liquids (PLAL) technique has been used to obtain Hydroxyapatite (HAp) suspensions nanoparticles from catfish bone. Catfish bone was used as natural source to prepare two targets at different calcination, sintering and pressing conditions. These targets were different in crystallinity, crystallite size and lattice parameters. All deposited HAp layers composed from HAp nanoparticles at range (20 - 100) nm as SEM images showed. The size of HAp nanoparticle depended on target's preparation conditions and deposition technique. XRD test confirmed the production of pure HAp. In vitro test proved the bioactivity of all deposited samples.

(Received October 01, 2018; Accepted June 3, 2019)

Keywords: Hydroxyapatite, Nanoparticles, Pulse laser ablation, Electrophoretic deposition and Drop casting technique.

1. Introduction

The problem with biomaterials is its low mechanical strength that restricts their use in situations where mechanical stress is existent. To overcome this problem different solutions have been proposed and studied. The production of a bioactive layer of calcium phosphate, bio composite and glass-ceramic and then coating the implants with these materials is one of these solutions. [1]

These bioactive materials mimic the behavior of natural bone and have properties so similar to natural bone that the osteoclasts (bone-dissolving cells) tear down these materials and replace them with natural bone.

In implant fabrication the most used calcium phosphate is HAp due to its excellent biocompatibility with skin, muscles, and hard tissues, also it do not exhibit any cytotoxic effects. HAp is a biological active material with multiple forms: coatings, particles, fibers, films, bio-composites which has wide biomedical applications. [2] HAp looks like human hard tissues in composition and morphology. It has the molecular structure of apatite with 39% by weight of Ca, 18.5% P and 3.38% of OH, with atomic ratio Ca/P is 1.67.

Extraction of HAp from natural sources, after appropriate thermal and chemical processing, can be considered as an important material for medical applications. [3] HAp material manufactured from animal bones seems to be an alternative for numerous products based on synthetic HAp. This important bio material has been extracted from bio sources, such as bones and teeth of big, fish bones, and bones of bovine. This extraction is low cost and environmentally favorite [4].

The biological apatite from marine animals such as fishes has low crystallinity and high content of effective trace element such as strontium, indicating its potential as bone substitute as well [5].

To date, nanomaterials have showed enhanced cytocompatibility and mechanical properties compared with respective conventional micronscale materials. The nano structural

*Corresponding author: mustafashh@yahoo.com

features, bioactive surfaces and favorable surface chemistry of nanomaterials which mimic bone significantly promote new bone formation compared with conventional materials. Thus these materials possibly serving as the next generation of orthopedic implant materials [6].

The utilization of nano biomaterials in bone grafting is more valuable than bulk materials, which leads to rapid and better tissue formation in the implant-bone interface [7].

In natural bone of human being HAp the nanometer size is considered to be essential for the mechanical properties of the bone. For the nano-sized ceramic materials; osteoblast adhesion and protein adsorption are higher than those of the customary micron-sized ceramic materials. For artificial bone substitution; nano crystalline HAp is frequently used to produce high quality HAp bioceramics [8].

The aim of this contribution is extraction of HAp nanoparticles from fish bone by pulse laser and deposition them on Ti substrate by two techniques.

2. Experimental part

Two procedures were applied to transform fish bones to powder. First one was mentioned By Mustafa et al.[9]. The milling process of first procedure was two steps: milling by food mixer and then by using milling machine type (Retczh PM40 Germany) to obtain fine fishbone. The milling duration by this machine was eight hours; the number of milling container rotation was 200 cycle/minute. To remove all organic materials; the powder was calcined at 800^0C for two hours inside tube furnace (Carbolite Type MTF 12/38A BAMFORD England). The powder then pressed under 13 ton to make pellet to be used as target with 1 cm diameter and then it was sintered at 800^0C for two hours. This pellet will be referred as (HApF1).

In the second procedure; fish bone's powder was obtained by direct mechanical peeling using electrical grinding machine. To remove all organic materials; the powder was calcined at 1000^0C for two hours. As soon as the calcination temperature had been reached, the sample will maintain cooled naturally in the furnace. The powder then pressed under 10 ton to make pellet to be used as (HApF2) with 1 cm diameter and then it was sintered at 1100^0C for four hours.

2.1. Laser ablation in liquid of HApF1 and HApF2

The target was put inside beaker, and then it was filled with 5 ml artificial ethanol. The sample was irradiated by Nd:YAG laser with following properties: Frequency(1Hz), Energy (150 mJ), Wavelength 1064 nm, number of pulse (55 , 120 and 1000)pulses. The distance between the sample and output laser aperture was (9 cm).

2.2. Deposition methods of ablation products

2.2.1. Drop casting method

The suspensions of ablated bones were dried onto Ti substrates by drop casting method. These substrates were heated to 100^0C before dropping process. Coated samples with ablated HAp were then annealed at 600^oC for 2h.

2.2.2. Electrophoretic deposition (EPD) method

This method was done using cell consisted from cathode (Ti disc) and anode (Ti substrate). The space between cathode and anode was 0.5 cm and filled with artificial ethanol. Different voltages were applied for variable time periods. During this electrical deposition the mixture was kept under continuous stirring. Coated samples by ablated HAp were then sintered in 600^0C for 2h.

2.3. Materials characterization

The crystalline nature of the materials, which were used in this study, was tested by powders X-ray Diffractometer using Cu Kα radiation. The 2Θ angles were swept in step of one degree. The indexing of the data was carried out using XRD Powder Diffraction Files (PDF), version 1992-1996, Ken Lagarec.

To identify the types of chemical bonds in a molecule Fourier transform infrared spectroscopy (FTIR) is used.

Surface morphologies of different surfaces were examined using scanning electron microscope SEM. To identify the elemental composition of a sample energy dispersive X-ray spectroscopy (EDS) is a suitable technique.

3. Results

3.1. Characterization of HApF1 and HApF2

3.1.1. XRD test of HApF1 and HApF2 powders

In order to test the best raw materials to extract HAp with best bioactivity catfish bones were good candidate to achieve this purpose. Two targets were prepared from the same fish bone but with different preparation conditions as was explained in experimental part. Fig. 1 shows XRD pattern of the powders of these two targets.

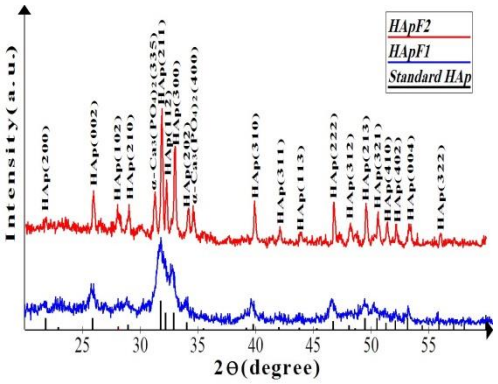

Fig. 1. XRD of HApF1 and HApF2 powders.

The data show that the peaks in XRD patterns of these powders match well with that of standard HAp, confirming that the material derived from catfish bones was HAp with existence of α-$Ca_3(PO_4)_2$ phase in the structure of HApF2 powder. Table 1 shows the differences between some calculated parameters from XRD patterns of the targets' powders. Crystallite sizes were calculated by using Scherrer's formula [10].

$$\text{Crystallite size} = \frac{0.9\,\lambda}{\beta\cos\theta} \tag{1}$$

where λ is X-ray beam wavelength (Å), β is full width at half maximum (rad) and Θ (^{0}) is Bragg's angle. a and c are hexagonal shape distances. These parameters are calculated using eq. 2 [11] and tabulated in Table 1.

$$\frac{1}{d^2} = \frac{4}{3}\left(\frac{h^2+hk+k^2}{a^2}\right) + \frac{l^2}{c^2} \tag{2}$$

where h, k, l = miller indices and d = distance between parallel indices.

Lattice volume for hexagonal shape = $(0.866)(a^2)(c)$

Table 1. Some differences between the properties of targets' powder.

Some physical parameters	HApF1	HApF2
Appearance of new phase other than Hap	Pure HAp phase	Beginning appearance of $Ca_3(PO_4)_2$ phase
Crystallinity degree (Xc)	31%	89%
Crystallite size (nm)	8.975	47.27
Lattice parameters: a(Å) / c(Å) / lattice volume(Å)^3	9.43/ 6.8878 / 530.4	9.4 / 6.85 / 524

The appearance of tricalcium phosphate Ca_3 $(PO_4)_2$ phase in XRD pattern of (HApF2) indicates the beginning decomposition of HAp [12]. Current lattice parameters are very close to that of standard HAp (a = 9.422 Å, c = 6.88Å, lattice volume = 528.9(Å)). Differences between two catfish targets will be important factor, among others, that affect directly on current study results.

3.1.2. FTIR test of HApF1 and HApF2 powders

Fig. 2 shows FTIR spectrums for the powders of two catfish targets and ablated HAp.

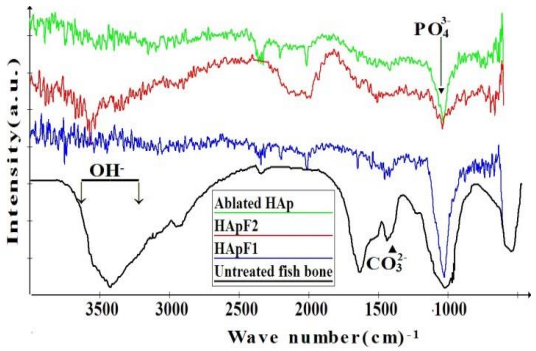

Fig. 2. FTIR spectra for HApF1 and HApF2 powders and ablated HAp.

The FTIR spectroscopy was measured to determine the various functional groups in the phosphate, hydroxyl and carbonate substitution in HAp. These spectra confirm that fish bone contains standard HAp due to the existence of the following group: OH^- (ν = 3571 cm^{-1}), PO_4^{3-}($\nu = 1050\ cm^{-1}$), and CO_3^{2-}peaks($\nu = 1453\ cm^{-1}$) [13, 14]. The intensities of CO_3^{2-}peaks decreased after calcination process, this refer to breaking organic materials inside catfish bones. Similar scenario is repeated for OH^- group for HApF1. After ablation there is no water inside ablated HAp.

3.1.3. Particle size distribution (PSD) of ablated HAp

Fig. 3 shows the differences in PSD between suspended HAp particles which were ablated from HApF1 and HApF2. These differences might attribute to the aggregation of HAp particles. This figure shows that the sizes of aggregate particles that ablated from HApF1 are greater than that ablated from HApF2 at the same ablated condition.

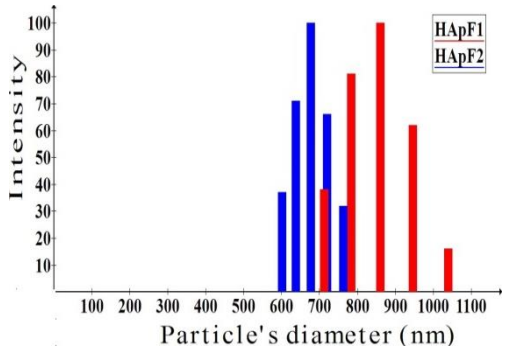

Fig. 3. Particle size distributions of HApF1 and HApF2 after PLAL process.

3.2. Characterization of HAp coatings

3.2.1. XRD test of HAp coatings

Fig. 4 shows XRD patterns of deposited HAp by drop casting method after ablation process for HApF1 and HApF2. XRD test was achieved after applying annealing process on deposited samples at 600^0C for two hours. Ma et al. confirmed that as the annealing temperature increased (from 1000 to 1300^oC) the HAp coating became denser [15]. However, a high temperature will cause the decomposition of HAp into undesirable α- and β-$Ca_3(PO_4)_2$ and then increasing in vitro dissolution and reducing biocompatibility [16]. To avoid decomposition of HAp coating the annealing in relatively moderate temperature was chosen (600^0C) in current work. The two patterns contain multi phases: Ti, TiO_2 and HAp phase. Ti phase appears because the substrate was Ti and the dominant peak (101) belongs to this phase. TiO_2 phase was created during deposition and annealing processes. This is in agreement with the result that obtained by Wong and Kwok[8]. HAp phase appears through eight peaks (002), (210), (211), (300), (202), (213) and (104). The clear presence of many reflections of HAp in Fig. 4, essentially matching the standard, demonstrates the formation of crystalline HAp particles. This is in agreement with that obtained by Parimal [17]. HAp phase is unchanged after deposition and annealing process This result is in agreement with that obtained by[8,17].Table 2 illustrates the comparison between some calculated parameters from the two curves in Fig. 4

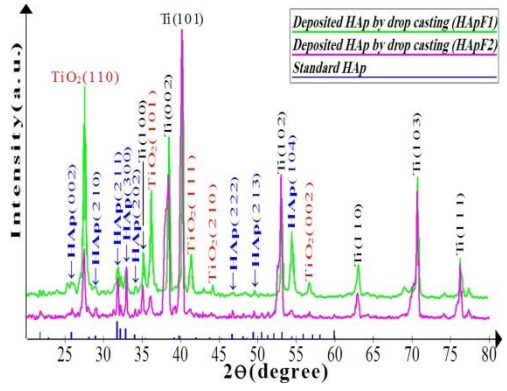

Fig. 4. XRD patterns of HAp coatings by drop casting.

The difference between crystallite size values in Table 2 decreased compare with that of the targets HApF1 and HApF2 in Table 1. The crystallinity degree of both deposited HAp by drop casting increased due to annealing process after deposition process.

Table 2. Some extracted parameters from Fig. 4.

Target	2Θ (degree)	Intensity (count/sec)	FWHM (degree)	Crystallite size (nm)	Crystallinity degree (Xc)
HApF1	31.741	86	0.2167	38	68%
HApF2	31.852	114	0.1625	50	94%

Fig. 5 shows XRD patterns of deposited HAp layer on Ti substrate by EPD method using two targets as source of HAp. The peaks that belong to HAp are weak.

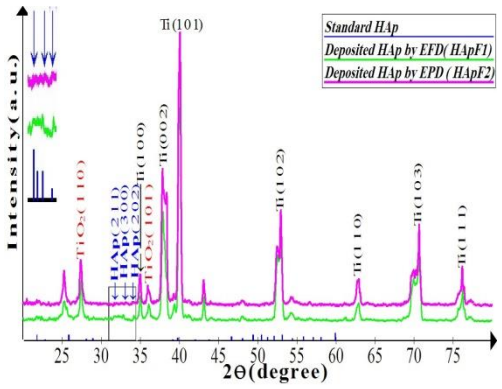

Fig. 5. XRD patterns HAp coatings by EPD. The inset shows weak peaks of HAp.

As the best of our knowledge there is no work had ablated HAp by laser from natural source and then deposited it by EPD technique.

3.2.2. SEM images of HAp coatings by EPD method

Fig. 6 shows SEM images of HAp coatings by EPD technique before and after annealing. These particles are prepared by using HApF1 and the conditions of EPD were (50 volt, 30 minute).

Image A in Fig. 6 confirms the formation of nano HAp particles during ablation process. After annealing, see image B, the appearance of nano particles begin to disappear and necking among the particles become obvious. This result is in agreement with that obtained by Onder Albayrak et al. [18].

By well observing image C in Fig. 6; one can note that the deposited layer closest to the substrate is collected from fine particles while the outer coating layers are composed of bigger particles. This can be explained by the fact that the smallest particles reached the highest electrophoretic velocity, therefor these were the preferential deposited. This result is in agreement with that obtained by Meng et al.[19].

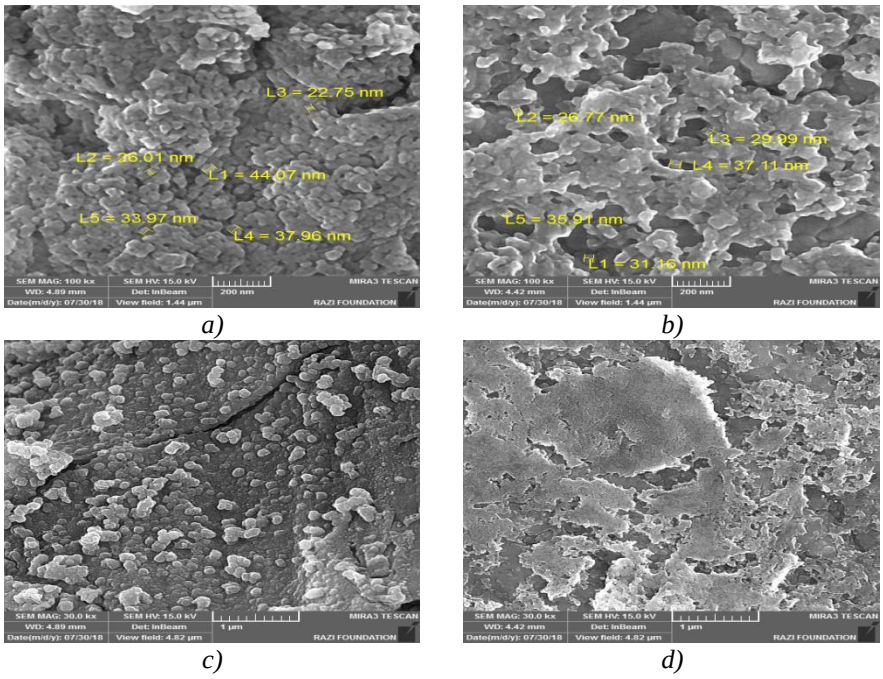

Fig. 6. SEM images of HAp coatings prepared by EPD technique before and after annealing using HApF1 target: a)before, b) after, c) before, d) after

After annealing individual nano particles disappear as shown in image D. In order to minimize their high free surface energy the smaller particles have a tendency to aggregate, resulting in densification and an increase in the grain size [20].

Fig. 7 shows SEM images of deposited HAp by EPD technique before and after annealing using HApF2 target as a source of apatite. These particles are prepared under the same ablation and EPD conditions that used for HApF1.

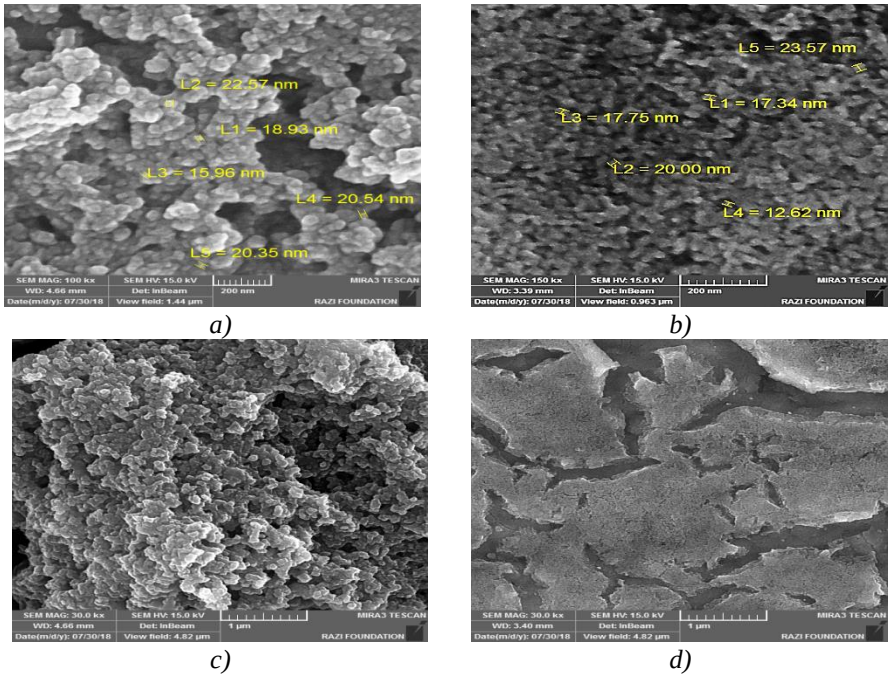

Fig. 7. SEM images of HAp coatings by EPD technique before and after annealing using HApF2 target:a)before, b) after, c) before, d) after

Appeared HApF2 layer in image G has good integrity with good packing.

Disappearance of nano particles after sintering is repeated after ablation, see A and B images of Fig. 6. Ablation and sintering processes has the same effect on the two prepared samples from catfish targets.

In spite of the aggregation of nanoparticles (appeared in image G of Fig. 7) it can be recognize these nanoparticles from each other. After annealing all these accumulations were disappeared as shown in image H. Comparison between image A in Fig. 6 with image E in figure 7 shows that the nano HAp particles in later image are smaller than that in former one. This result might due to preparation conditions of HApF1 and HApF2 where the pressure and sintering temperature higher for HApF2.

After annealing; the connections between nano HAp particles (prepared by using HApF2 are not strong compared with that prepared by using HApF1 (compare image B with image F).

Webster et al. proved that the bioactivity had enhanced through the nano crystalline formation, due to the HAp nano coating [21]. So keeping the nanoparticles with their nano sizes after annealing will play important rule in construction of HAp during biomimetic process.

After annealing; many cracks are formed in the body of HAp layer due to the mismatching of thermal expansion coefficient between this layer and Ti substrate, see image H . The formation of micro-cracks during heating and cooling was also occurred during Wei et al [22] study which included deposition of HAp on Ti6Al4V alloy by EPD technique.

3.2.3. SEM images of HAp coating by drop casting method

Fig. 8 shows SEM images of deposited HAp on Ti substrate by drop casting method before and after annealing. These particles are prepared by using HApF1 under the following ablation conditions (150mj, 55pulse). Image I in Fig. 8 shows that the HApF1 particles have larger diameters compare with that obtained by the EPD method for the same target. After annealing the boundaries of these particles begin to disappear and there is a merging between them to form semi continuous layer, see image J. Also the comparison between the images K with image L in this figure proves the disappearance of vacancies after annealing.

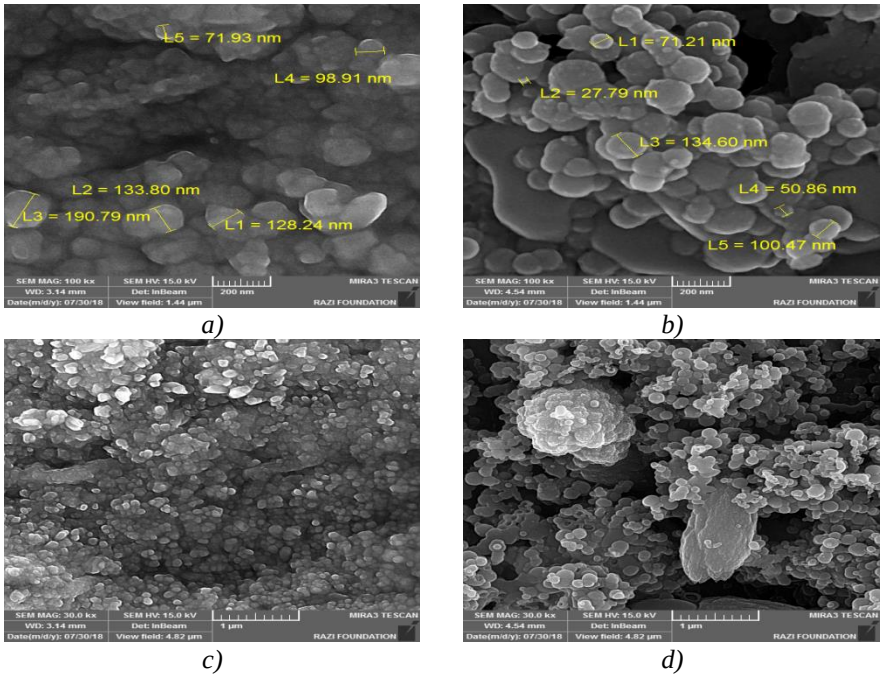

Fig. 8. SEM images of HAp coating using drop casting method before and after annealing using HApF2 target: a)before, b) after, c) before, d) after

Fig. 9 shows SEM images of HAp coating on Ti substrate by drop casting method before and after annealing. These particles are prepared by using HApF2 under the same ablation conditions used for HApF2.

Fig. 9 shows images of relatively large deposited HAp particles by drop casting technique using HApF2. Before annealing most of HAp particles' sizes were in micro scale. After annealing the sizes of particles become larger and the pores still exist.

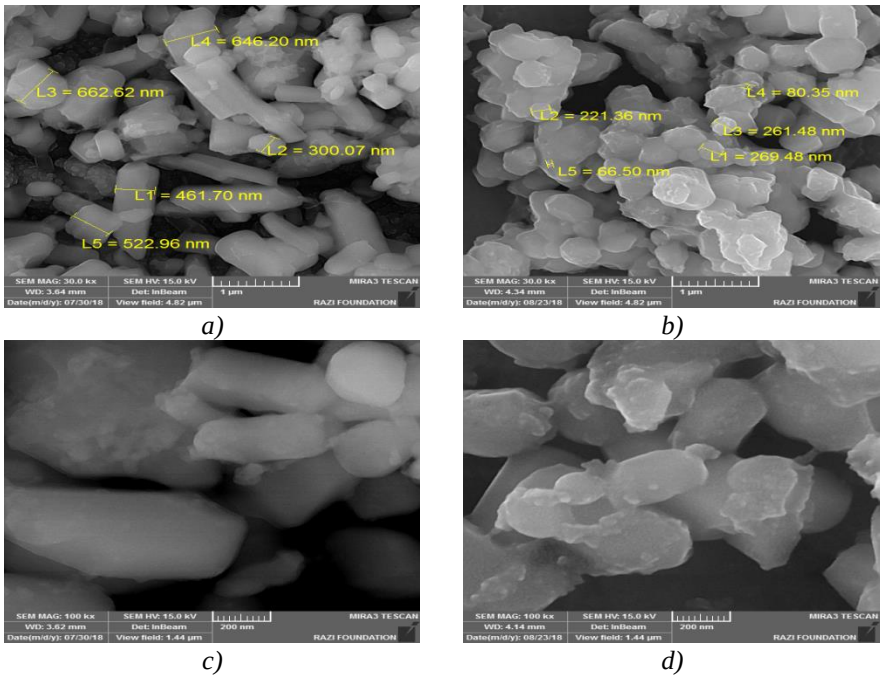

Fig. 9 SEM images of HAp coating using drop casting method before and after annealing using HApF2 target: a)before, b) after, c) before, d) after

3.2.4. Calcium to phosphorus (Ca/p) molar ratios

The results in Table 3 show the tendency of the Ca/P molar ratio to increase with increasing annealing temperature.

Table 3. Shows Ca/p molar ratios for HAp coatings by EPD and drop casting methods.

Target	Deposition method	Before annealing	After annealing
HApF1	EPD	1.49	1.87
	Drop casting	1.37	1.67
HApF2	EPD	1.01	17.5
	Drop casting	1.29	1.53

At temperatures in the range of 500-900^{0}C, the OH^- bonds are easily broken and become detached from the HAp structure [23]. This causes a rapid evaporation or oxidation of the P element in HAp structure [22]. Stable HAp phases correspond to Ca/P ratio within a range of (1.3–1.8). The highest increase of Ca/P ratio to 17.5 can be attributed to the diffusion of phosphorus ions, resulting in the partial HAp decomposition [24]. The increasing Ca/p ratios in agreement with that obtained by Sobczak et al [3].

3.6. Bioactivity of HAp coatings by biomemitic technique

3.6.1. XRD test of formed bone like apatite (BHAp) on HAp coatings

Two samples were tested to exam their bioactivities: formed bone like apatite on deposited HAp by EPD using target1 (BHApF1) and target 2 (BHApF2) respectively. Fig. 10 shows XRD patterns of both BHApF1 and BHApF2. The dominant peak (211) for XRD pattern of BHApF2 belongs to hydroxyapatite phase. This result is a strong evidence for excellent bioactivity for this sample. Also the same peak appears for the second curve BHApF1 in Fig. 10 but with lower intensity indicating to lower bioactivity. This result shows the superiority of HApF2 on HApF1.

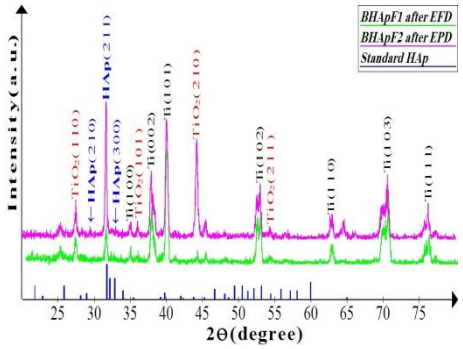

Fig. 10. XRD patterns of BHApF1 and BHApF2.

Table 4 shows the higher intensity of BHApF2 compare with that of BHApF1.

Table 4. Some extracted parameters from XRD patterns in Fig. 10.

Sample	2Θ (degree)	Intensity (counts)	FWHM (degree)	Crystallite size (nm)
BHApF1	31.709	26	0.275	30
BHApF2	31.684	132	0.203	40.5

Fig. 11 shows XRD patterns of BHApF1 and BHApF2 that formed on deposited HAp by drop casting technique using target1 and target2 respectively.

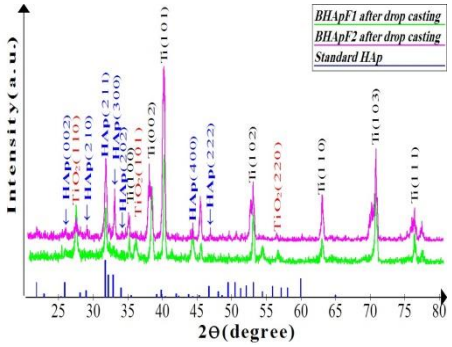

Fig. 11. XRD patterns of BHApF1 and BHApF2 after soaking HAp coatings by drop casting in SBF.

Seven peaks belong to HAp phase can observe in XRD pattern of BHApF2 in Fig. 11. The same peaks formed for the BHApF1 sample but with different intensities. Table 5 shows

comparison between some parameters that calculated from these two curves. The crystallinity degree of BHApF2 is higher indicating to its better bioactivity.

Table 5. Some extracted parameters from Fig. 11.

Sample	2Θ (degree)	Intensity (counts)	FWHM (degree)	Crystallite size (nm)	crystallinity degree
BHApF1	31.7552	40	0.2667	30.9	56%
BHApF2	31.8475	63	0.33140	24.9	88%

All samples shown in figures 10 and 11 have variable bioactivities due to the formation of HAp on their surfaces. There is no any evidence of other phases of calcium phosphate or impurities.

4. Discussions

Nissan confirmed that the appearance of nanoparticles enhances the bioactivity [25]. The release of calcium ions from nano HAp is similar to that from biological apatite. Nano HAp has higher surface area and surface roughness resulting in better cell adhesion and cell–matrix interactions [26]. Dong et al. showed that ceramic biomaterials based on nano-sized HAp enhanced resorb ability [27-28] and increase bioactivity [29-30].

In current work the enhancement of the bioactivity was represented by the formation of BHApF1 and BHApF2 layers as result to deposition of nan HAp on Ti substrate. The formation of bone like apatite is in agreement with the result that obtained by Kwok et al. [31].

It is important to distinguish between the properties of HAp coating and formed BHAp on them. HAp coating must have special merits to produce apatite layer that built strong bonds with bone.

The dissolution of the amorphous phases causes super saturation of Ca and P ions in the physiological media causing reprecipitation of a crystallized phase. Also, amorphous HAp undergoes rapid dissolution in the physiological environment but highly crystalline HAp coatings show low dissolution rates [32]. Donglu et al. confirmed that the bioactivity is reduced at higher degree of crystallinity [33].

So before implantation process it is important to coat the implant with HAp that has amorphous phase or mixture contain both amorphous and crystalline phases.

After implantation it is desirable to create crystalline BHAp that undissolved in human blood and have all natural bone properties. Crystalline coatings are observed to be more adherent to Ti substrates [34]. Besides, HAp with low crystallinity quickly becomes weak and may promote inflammatory responses. It is therefore desirable to have a high degree of crystallinity in BHAp [35].

By applying above conditions on produced samples deposited HAp by EPD (for both targets) were the best samples because they have amorphous phase before in vitro and relatively high crystallinity after this test, see Fig. 12.

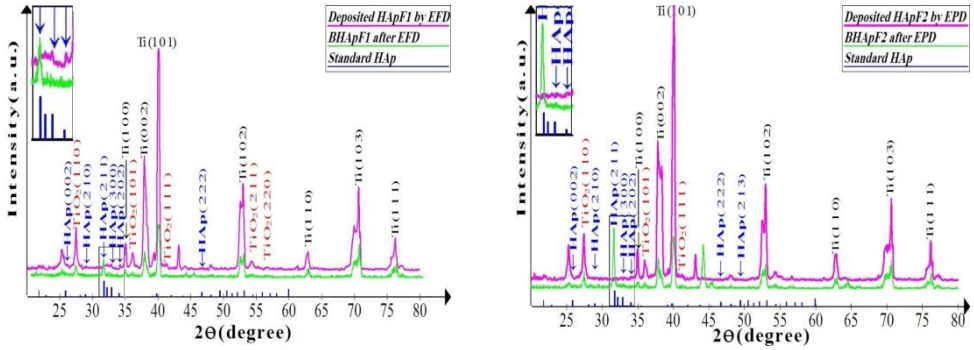

a) *b)*

Fig. 12. XRD patterns of HAp coatings by EPD before and after in vitro test: A (HApF1) and B (for HApF2).

Deposited HAp by drop casting using target2 might not dissolve to create new HAp but instead a new BHApF2 layer was formed on it. XRD patterns in Fig. 13 shows the existence of the same three major peaks before and after in vitro test. The presence of these peaks with approximately the same intensities and the same (2Θ) positions might refer to the likelihood between old and new HAp layer. The first layer was most likely not dissolved to create the new layer but instead it enhanced forming new one on it.

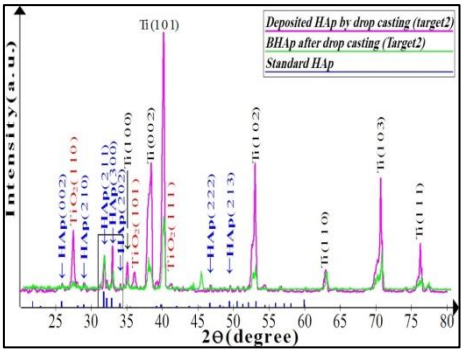

Fig. 13. XRD patterns of HAp_{F2} coatings by drop casting before and after in vitro test.

4.1. SEM images of BHAp samples

Fig. 14 clarifies SEM images of formed BHAp by biomemitic process. Image D shows both old and new apatite.

Image C illustrates typical cauliflower morphology of BHAp. This figure looks like one obtained by [36].

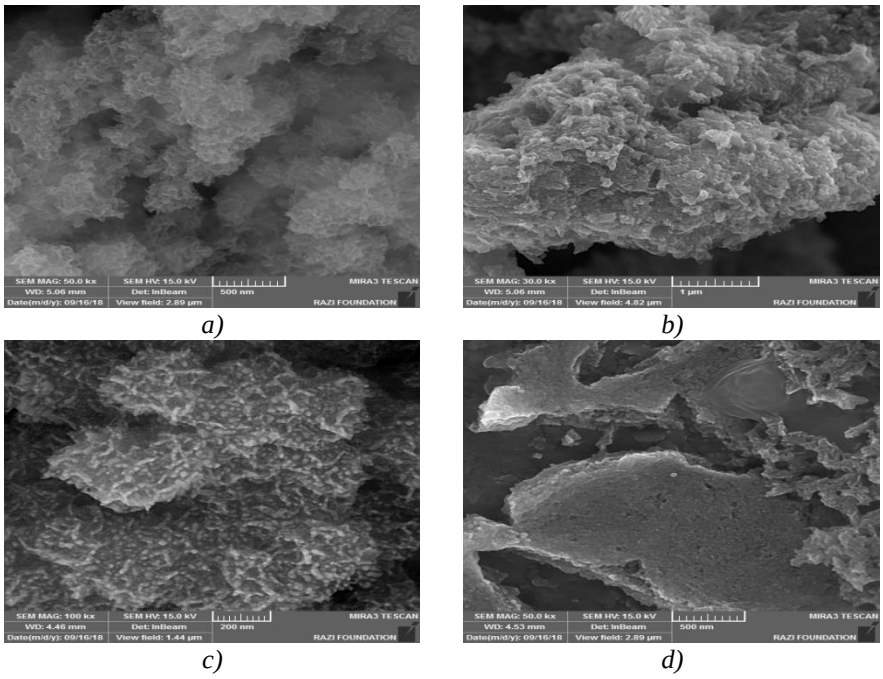

Fig. 14. SEM images of formed BHAp on deposited HAp by EPD:
(A and B for BHApF1), (C and D for HApF2).

Fig. 15 shows SEM images of formed BHAp on deposited HAp by drop casting method. All images illustrate two layers before and after immersion in SBF. Produced BHAp particles have small sizes compare with that before biomimetic process.

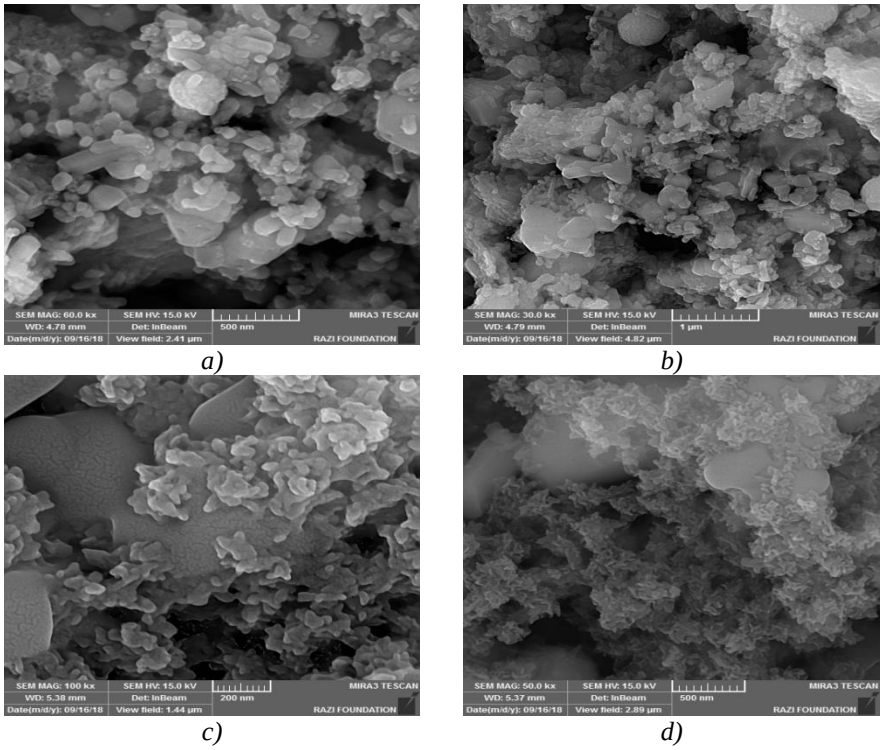

Fig. 15. Second SEM image of formed BHAp on HAp coating by drop casting:
for HApF2 .

The appearance of BHAp in all images in above four figures proves the bioactivity of these samples.

4.2. Ca/P ratios of formed BHAp

Table 6 shows the reduction of Ca/P ratios for all samples. This decrease may be attributing to precipitation of a non-stoichiometric HAp from SBF. This result is in a good agreement with the earlier report that had written by Kaygili et al. [37].

Table 6. Molar ratio Ca/P before and after biomimetic process.

Target	HAp Coating	Ca/P ratio of deposited HAp	Ca/P ratio of BHAp
HApF1	HAp (EPD)	1.87	1.26
	HAp (drop casting)	1.67	1.37
HApF2	HAp (EPD)	17.5	1.46
	HAp (drop casting)	1.53	1.29

5. Conclusions

The conditions of targets' preparation and the type of deposition technique were crucial factors that effect on the properties of deposited HAp and formed BHAp.

References

[1] E. C. D. S. Rigo, et al., Materials Research **11**(1), 47(2008).
[2] A. A. El Hadad, et al., Materials **10**(2), 94(2017).
[3] A. Sobczak-Kupiec, et al., Bulletin of Materials Science **36**(4), 755(2013).
[4] I. Hilmi, M. Rinastiti, M. Herliansyah, Instrumentation, Communications, Information Technology, and Biomedical Engineering (ICICI-BME), 2nd International Conference on. 2011. IEEE.
[5] Q. Liu, et al., BioMed Research International **2013** (2013).
[6] L. Zhang, et al., International Journal of Nanomedicine **3**(3), 323(2008).
[7] M. Boutinguiza, et al., Physics Procedia **12**, 54 (2011).
[8] P. Wong, C. Kwok, Medical Device Materials IV: Proceedings of the Materials & Processes for Medical Devices Conference 2007, Palm Desert, California, USA. 2008. ASM International.
[9] M. Sh. AlHilfi, A. Yahya Alhijazi, Th. L. Alzubaydi, A. H. Al-Fouadi, Journal of Natural Science Research **4**(2), (2014).
[10] H. P. Klug, L. E. Alexander, X-Ray Diffraction Procedures: For Polycrystalline and Amorphous Materials, 2nd Edition, by Harold P. Klug, Leroy E. Alexander, pp. 992. ISBN 0-471-49369-4. Wiley-VCH, May 1974, 1974: p. 992.
[11] A. F. Hasa, A. H. K. Ltaief, J. F. Hamodi, Engineering and Technology Journal **33**(6 Part (B) Scientific), 1003 (2015).
[12] K. Prabakaran, S. Rajeswari, Trends Biomater Artif Organs **20**(1), 20 (2006).
[13] A. Afshar, et al., Materials Science and Engineering **128**(1-3), 243 (2006).
[14] J. Davies, International Journal of Prosthodontics **11**(5), (1998).
[15] J. Ma, et al., Nanotechnology**14**(6), 619 (2003).
[16] J. Ma, et al., Journal of Materials Science: Materials in Medicine **14**(9), 797 (2003).
[17] M.Wei, A. Ruys, B. Milthorpe, C. Sorrell, and J. Evans, Journal of Sol-Gel Science and Technology.**21**,39(2001).
[18] O. Albayrak, et al., Rev. Adv. Mater. Sci. **15**, 10 (2007).
[19] X. Meng, T.-Y. Kwon, K.-H. Kim, Dental Materials Journal **27**(5), 666 (2008).

[20] E. Landi, A.Tampieri, G. Celotti, and S. Sprio, Journal of the European Ceramic Society, . **20**, 2377(2000).
[21] T. J. Webster, et al., Biomaterials **22**(11), 1327 (2001).
[22] M. Wei, A. Ruys, B. Milthorpe, and C. Sorrell, Journal of Materials Science: Materials in Medicine. **16**(4), 319(2005).
[23] Mustafa Sh. Hashim, thesis, Surface modification of Ti alloys by coating with Iraqi fishbone to enhance osseointegration and improve corrosion resistance (in vitro and in vivo study) Al – Mustansiriya University, 2014, Baghdad, Iraq.
[24] D. Wang, C. Chen, J. Ma, and T. Lei, Aplied Surface Science. **253**,4016(2007).
[25] B. Ben-Nissan, Current opinion in solid state and materials science **7**(4-5), 283 (2003).
[26] L. F. Boesel, et al., Acta Biomaterialia **3**(2), 175 (2007).
[27] Z. Dong, Y. Li, Q. Zou, Applied Surface Science **255**(12), 6087 (2009).
[28] Y. Wang, L. Liu, S. Guo, Polymer Degradation and Stability **95**(2), 207 (2010).
[29] Y. Cai, et al., Journal of Materials Chemistry **17**(36), 3780 (2007).
[30] S. V. Dorozhkin, Acta Biomaterialia **6**(3), 715 (2010).
[31] C. Kwok, et al., Applied Surface Science **255**(13-14), 6736 (2009).
[32] D. H. Kim, et al., Journal of the American Ceramic Society **86**(1), 186 (2003).
[33] D. Shi, G. Jiang, J. Bauer, Journal of Biomedical Materials Research: An Official Journal of The Society for Biomaterials, The Japanese Society for Biomaterials, and The Australian Society for Biomaterials and the Korean Society for Biomaterials, **63**(1), 71 (2002).
[34] M. Komath, et al., Bulletin of Materials Science **34**(2), 389 (2011).
[35] P. Choudhury, D. Nanomedicine. Elsevier 84 (2012).
[36] L. F. Boesel, et al., Acta Biomaterialia **3**(2), 175 (2003).
[37] O. Kaygili, et al., Progress in Biomaterials **5**(3-4), 173 (2016).